UCRL-ID-121836

DSI3D — RCS Test Case Manual

Niel Madsen
David Steich
Grant Cook
Bill Eme

August 1995

Lawrence Livermore National Laboratory

This work was performed under the auspices of the U. S. Department of Energy by Lawrence Livermore National Laboratory under contract No. W-7405-Eng-48.

DSI3D - RCS

Test Case Manual

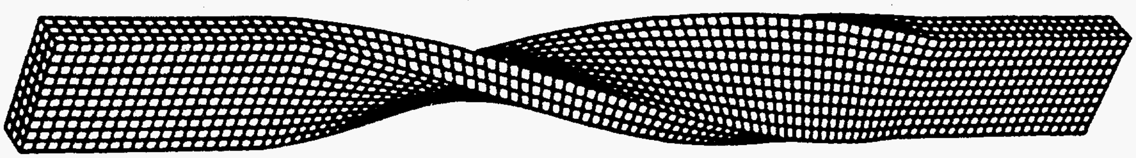

Niel Madsen, David Steich, Grant Cook, Bill Eme

Lawrence Livermore National Laboratory

Table of Contents

Introduction

The DSI3D-RCS code is designed to numerically evaluate radar cross sections on complex objects by solving Maxwell's curl equations in the time-domain and in three space dimensions. The code has been designed to run on the new parallel processing computers as well as on conventional serial computers.

The DSI3D-RCS code has been used to solve the following problems:

- Wedge Cylinder - thin flat metal plate
- Wedge Cylinder with Plate extension - thin flat metal plate
- Plate with Half Cylinder Extension - thin flat metal plate
- Rectangular Plate (Business Card) - thin flat metal plate
- Wedge Cylinder with Gap - thin flat metal plate
- NASA Almond
- Wavelength Circular Cavity

In order to generate each of the angle sweeps, it was necessary to run DSI3D once for each data point on the graphs. This is because these are backscatter calculations, and the incident pulse comes from a different direction as the angle ϕ is changed. To automate the process of performing all of these simulation runs, we used the following shell script:

```
#!/bin/csh
########################################################################
#
#>  emcc.csh - CSH script to make phi varying d3d runs on meiko
#>
#>  Usage:
#>    csh emcc.csh
#>
#>  Comments
#>    This script automates the process of time iterating psre
#>    problems and collecting the resulting time history data into
#>    an ULTRA format ASCII file.
#>
########################################################################

set cnt=-1


set phi=-1
set realphi = -1
```

```
#......................................... iterate runs until done
date
while ($cnt < 180)
      @ cnt += 1
      @ phi = 2 * $cnt
        if ($cnt > 90) @ phi -= 181
      @ realphi = 180 - $phi

#       ......................................... set up first/next run
      sed   -e "/PHI/s//${phi}/" paramsPHI.dat.hh >params.dat

      echo "Running problem > target2 HH $cnt $phi $realphi"

      rm rest* tp* dum.${realphi}.hh ul.${realphi}.hh
      prun -v  -pp0  -n64 -b0 ~beme/dsi3d/emcc/predsi3d
      date
      prun -v  -pp0  -n64 -b0 ~beme/dsi3d/emcc/dsi3d
      date
#     cat tp* >dum.${realphi}.hh
      prun -v  -pp0  -n64 -b0 ~beme/dsi3d/emcc/rcss
        mv ultra.out ul.${realphi}.hh
      date
end
```

Wedge Cylinder

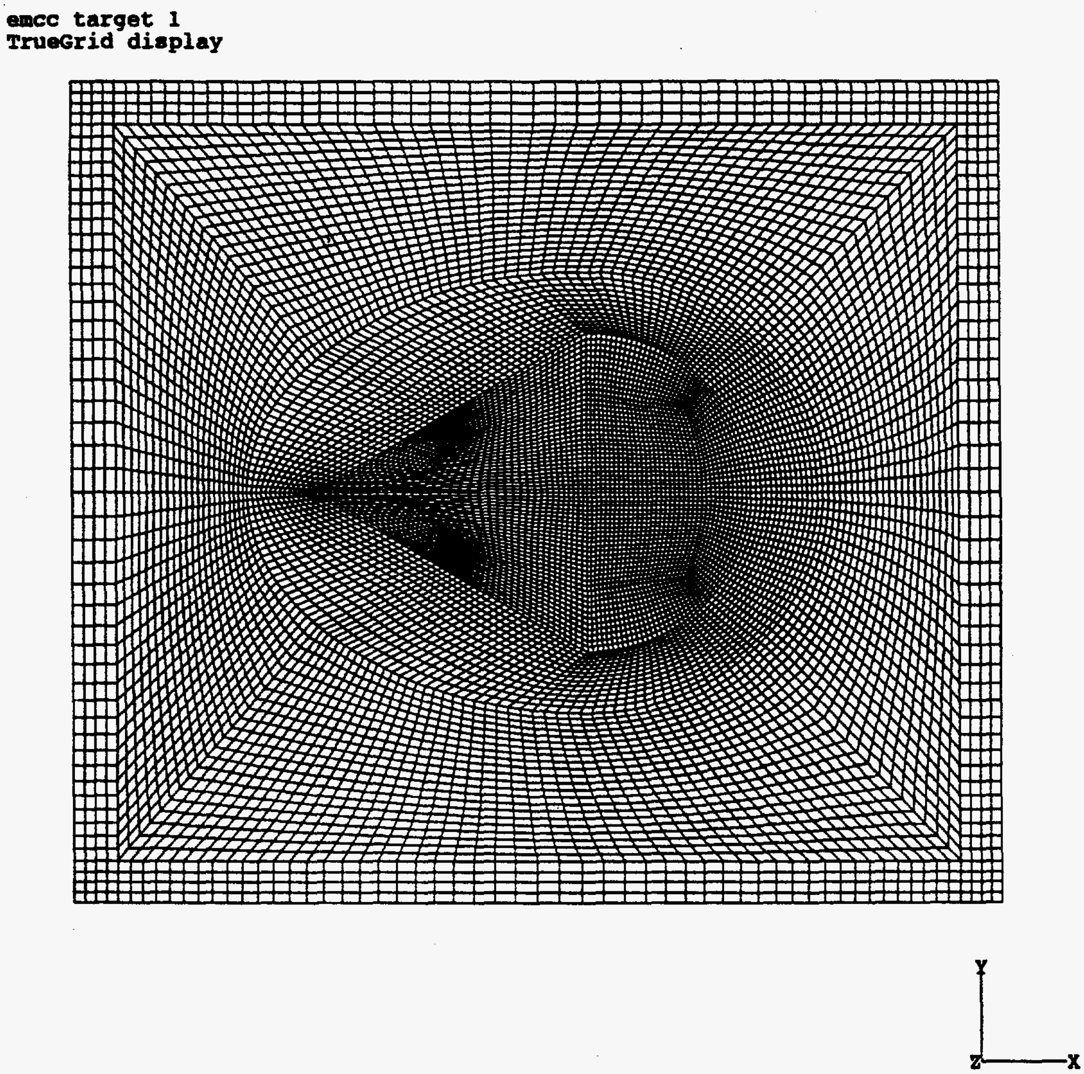

Figure 1. View of the target 1 mesh looking down the z-axis. Each cut of the mesh at a constant z coordinate in the mesh has this same appearance. See Figure 2. for the distribution of nodes in the z direction.

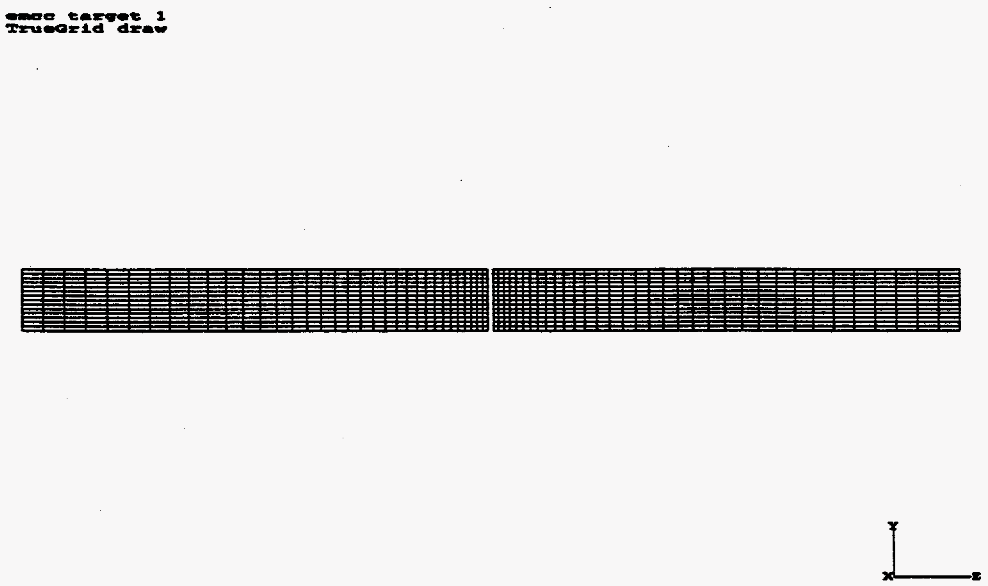

Figure 2. The distribution of nodes in the z direction for each of the planar targets (1-5).

The following input file was used with the shell script given in the introduction to obtain the results in Figure 3. Note the use of the pattern **PHI** that the shell script sets to a valid integer.

```
local_dir     /var/tmp/t1_
start_time    0.0
num_steps     8192
dt            0.0
eps0          8.8541853367e-12
xmu0          1.2566e-06
driver_id     7
alpha         30
ascii_coef    0
restarts      500

driver 80.0   PHI.0 90.0 78721.56184 0.1898598 85.0 16.0 0.0 2.0 -1.0

primary_output_edges
780 915
915 930

rbc higdon_higdon  60 0.0 0.01 10.0 0.015

FARREF  0.0  0.0  0.0

FARPOL
   0.0
   90.0

FARPTS
   80.    PHI.0    0.
```

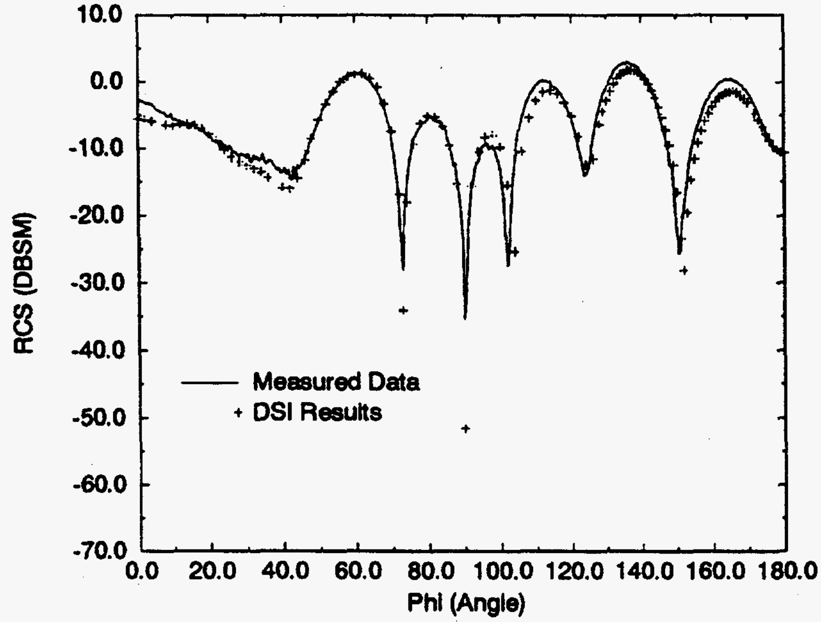

Figure 3. HH polarization cross section at 5.9 GHz for target 1, using the mesh in Figures 1 and 2.

A slightly different input file was used with the shell script given in the introduction to obtain the results in Figure 4. As seen below, the only difference is in the polarization used in the **driver** command. Again, note the use of the pattern **PHI** that the shell script sets to a valid integer.

```
local_dir     /var/tmp/t1_
start_time    0.0
num_steps     8192
dt            0.0
eps0          8.8541853367e-12
xmu0          1.2566e-06
driver_id     7
alpha         30
ascii_coef    0
restarts      500

driver 80.0   PHI.0 0.0 78721.56184 0.1898598 85.0 16.0 0.0 2.0 -1.0

primary_output_edges
780 915
915 930

rbc higdon_higdon  60 0.0 0.01 10.0 0.015
```

```
FARREF  0.0  0.0  0.0

FARPOL
   0.0
   90.0

FARPTS
   80.    PHI.0    0.
```

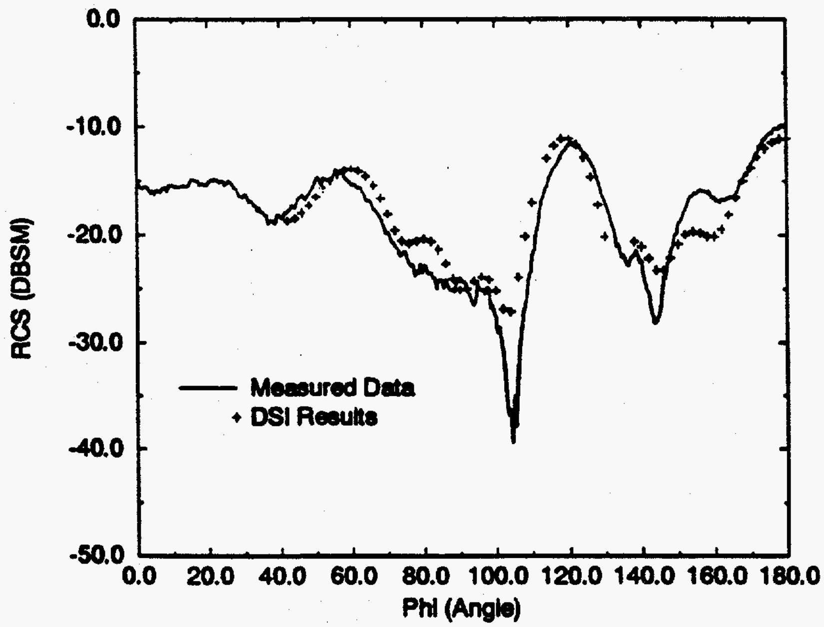

Figure 4. VV polarization cross section at 5.9 GHz for target 1, using the mesh in Figures 1 and 2.

Wedge Cylinder with Plate Extension

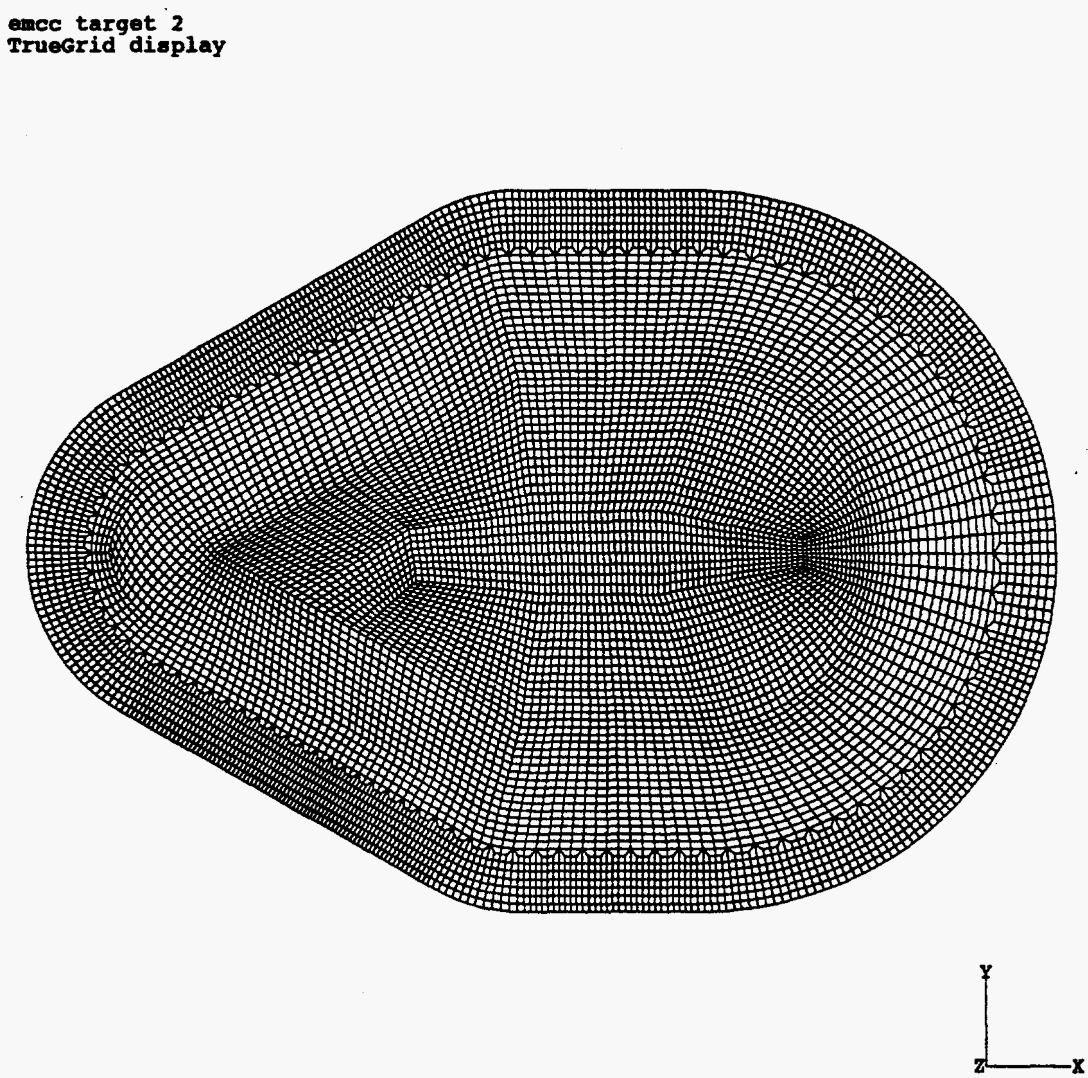

Figure 5. View of the target 2 mesh looking down the z-axis. Each cut of the mesh at a constant z coordinate in the mesh has this same appearance. See Figure 2 for the distribution of nodes in the z direction.

The following input file was used with the shell script given in the introduction to obtain the results in Figure 6.

```
local_dir     /var/tmp/t2_
start_time    0.0
num_steps     8192
dt            0.0
eps0          8.8541853367e-12
xmu0          1.2566e-06
driver_id     7
alpha         30
ascii_coef    0
restarts      500

driver 80.0   PHI.0 90.0 78721.56184 0.1898598 85.0 16.0 0.0 2.0 -1.0

primary_output_edges
780 915
915 930

rbc higdon_higdon  60 0.0 0.01 10.0 0.015

FARREF  0.0  0.0  0.0

FARPOL
   0.0
   90.0

FARPTS
   80.    PHI.0    0.
```

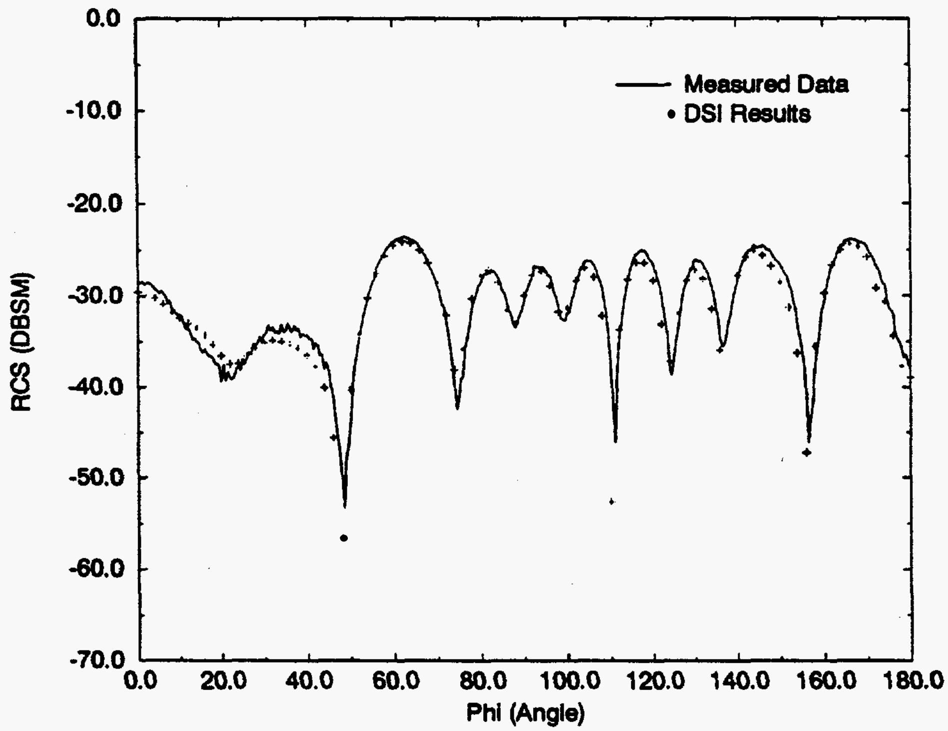

Figure 6. HH polarization cross section at 5.9 GHz for target 2, using the mesh in Figures 5 and 2.

The same input file that was used for Figure 4 is also used to obtain Figure 7.

```
local_dir     /var/tmp/t2_
start_time    0.0
num_steps     8192
dt            0.0
eps0          8.8541853367e-12
xmu0          1.2566e-06
driver_id     7
alpha         30
ascii_coef    0
restarts      500

driver 80.0   PHI.0 0.0 78721.56184 0.1898598 85.0 16.0 0.0 2.0 -1.0
```

```
primary_output_edges
780 915
915 930

rbc higdon_higdon  60 0.0 0.01 10.0 0.015

FARREF  0.0  0.0  0.0

FARPOL
   0.0
   90.0

FARPTS
   80.    PHI.0    0.
```

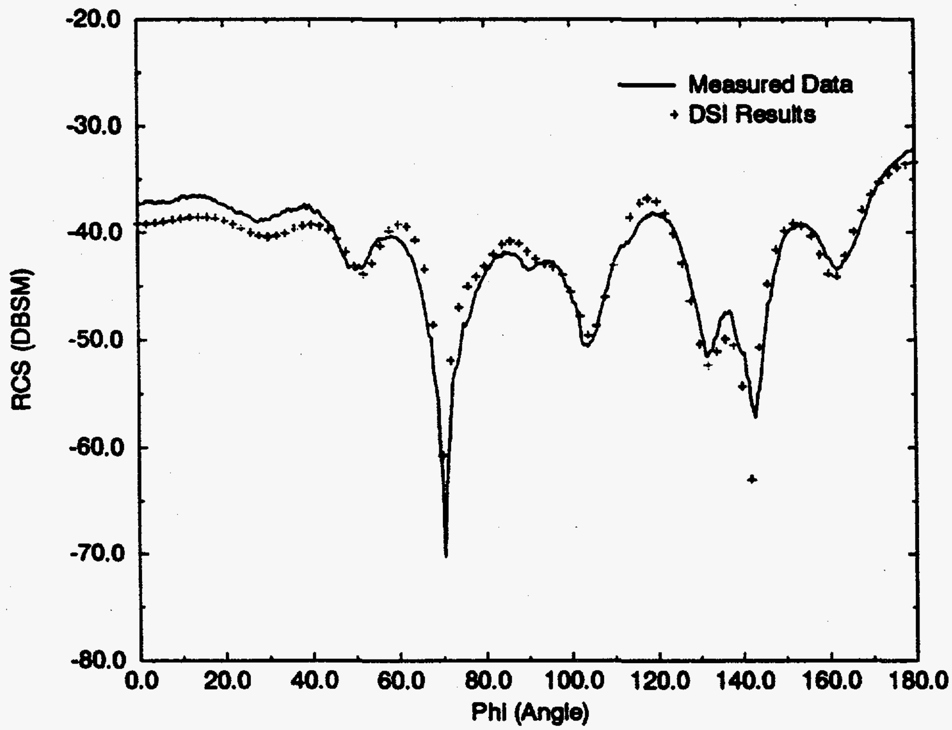

Figure 7. VV polarization cross section at 5.9 GHz for target 2, using the mesh in Figures 5 and 2.

Plate with Half Cylinder Extension

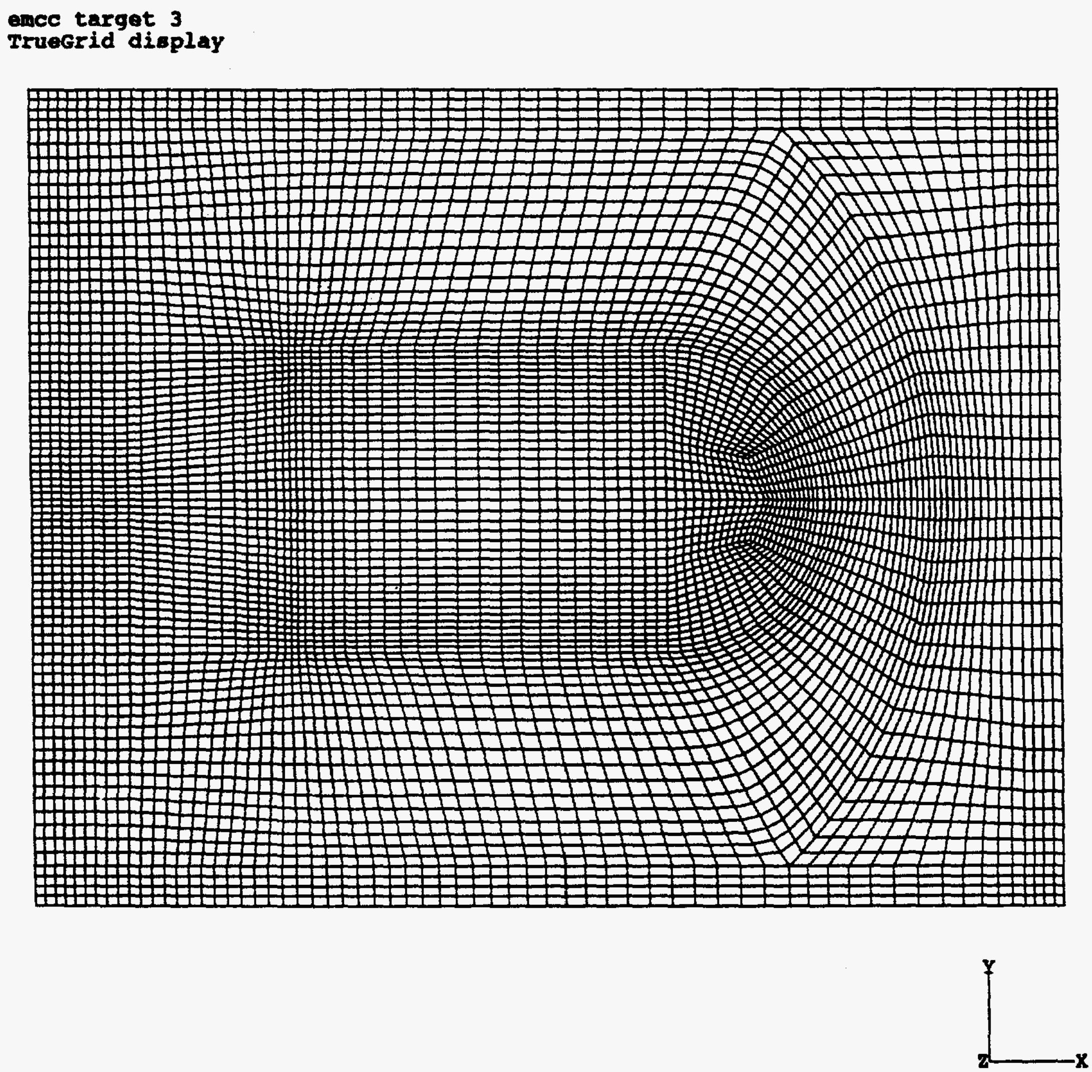

Figure 8. View of the target 3 mesh looking down the z-axis. Each cut of the mesh at a constant z coordinate in the mesh has this same appearance. See Figure 2 for the distribution of nodes in the z direction.

The same input file that was used for Figure 3 is also used to obtain Figure 9.

```
local_dir     /var/tmp/t3_
start_time    0.0
```

```
num_steps     8192
dt            0.0
eps0          8.8541853367e-12
xmu0          1.2566e-06
driver_id     7
alpha         30
ascii_coef    0
restarts      500

driver 80.0   PHI.0 90.0 78721.56184 0.1898598 85.0 16.0 0.0 2.0 -1.0

primary_output_edges
780 915
915 930

rbc higdon_higdon  60 0.0 0.01 10.0 0.015

FARREF  0.0  0.0  0.0

FARPOL
   0.0
   90.0

FARPTS
   80.    PHI.0    0.
```

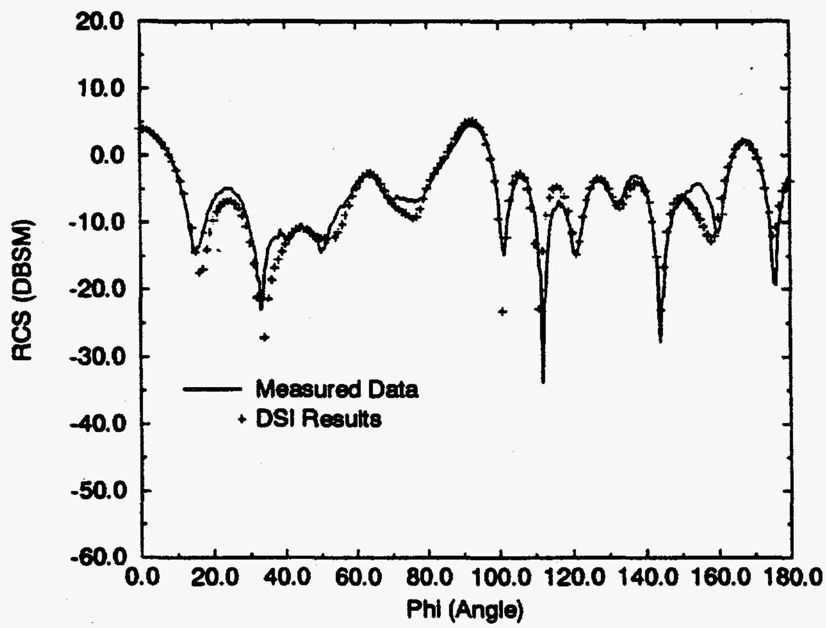

Figure 9. HH polarization cross section at 5.9 GHz for target 3, using the mesh in Figures 8 and 2.

The same input file that was used for Figure 4 is also used to obtain Figure 10.

```
local_dir     /var/tmp/t3_
start_time    0.0
num_steps     8192
dt            0.0
eps0          8.8541853367e-12
xmu0          1.2566e-06
driver_id     7
alpha         30
ascii_coef    0
restarts      500

driver 80.0   PHI.0 0.0 78721.56184 0.1898598 85.0 16.0 0.0 2.0 -1.0

primary_output_edges
780 915
915 930

rbc higdon_higdon  60 0.0 0.01 10.0 0.015

FARREF  0.0  0.0  0.0

FARPOL
   0.0
   90.0

FARPTS
   80.    PHI.0    0.
```

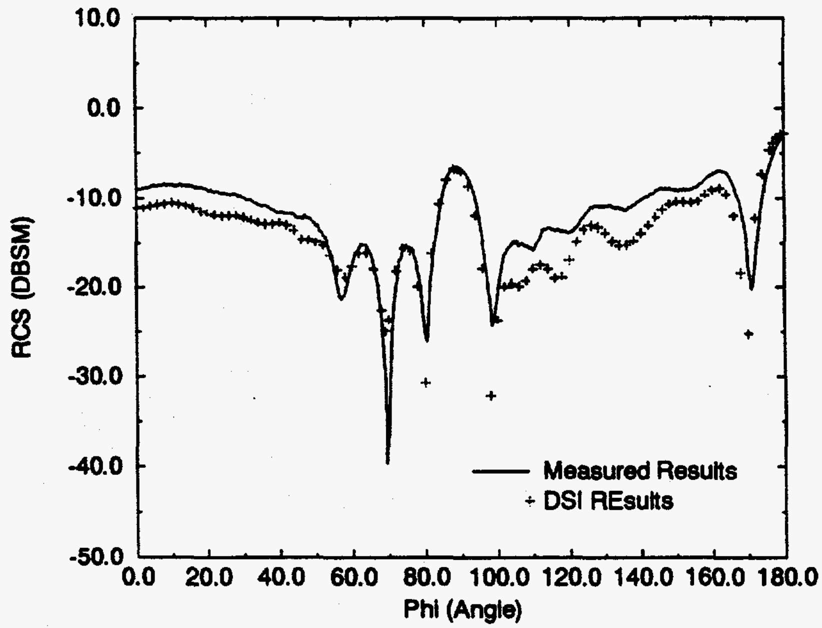

Figure 10. VV polarization cross section at 5.9 GHz for target 3, using the mesh in Figures 8 and 2.

Rectangular Plate

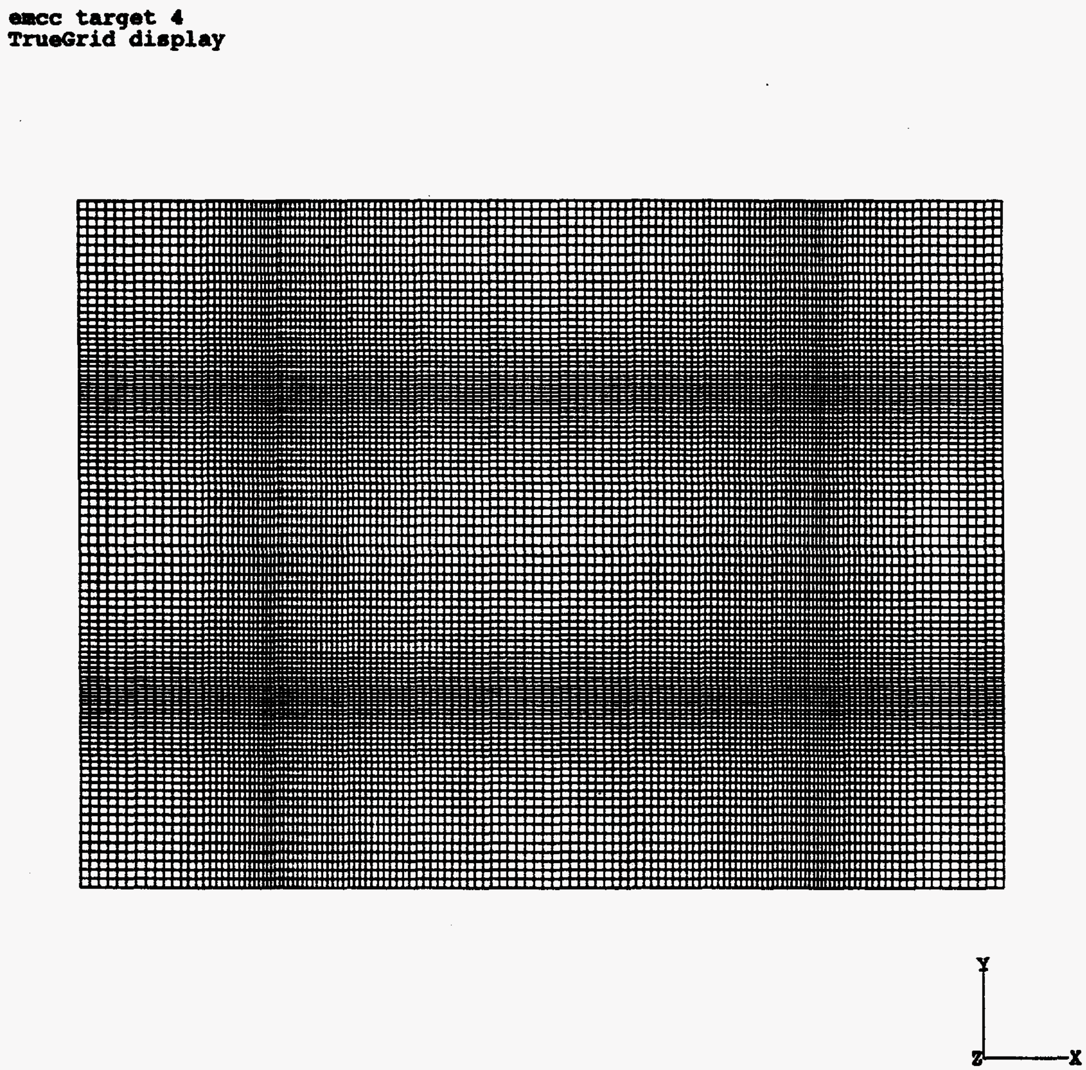

Figure 11. View of the target 4 mesh looking down the z-axis. Each cut of the mesh at a constant z coordinate in the mesh has this same appearance. See Figure 2 for the distribution of nodes in the z direction.

The same input file that was used for Figure 3 is also used to obtain Figure 12.

```
local_dir     /var/tmp/t4_
start_time    0.0
num_steps     8192
```

```
dt              0.0
eps0            8.8541853367e-12
xmu0            1.2566e-06
driver_id       7
ascii_coef      0
restarts        500

driver 80.0   PHI.0 90.0 78721.56184 0.1898598 85.0 16.0 0.0 2.0 -1.0

primary_output_edges
780 915
915 930

rbc higdon_higdon  60 0.0 0.01 10.0 0.015

FARREF  0.0  0.0  0.0

FARPOL
   0.0
   90.0

FARPTS
   80.    PHI.0    0.
```

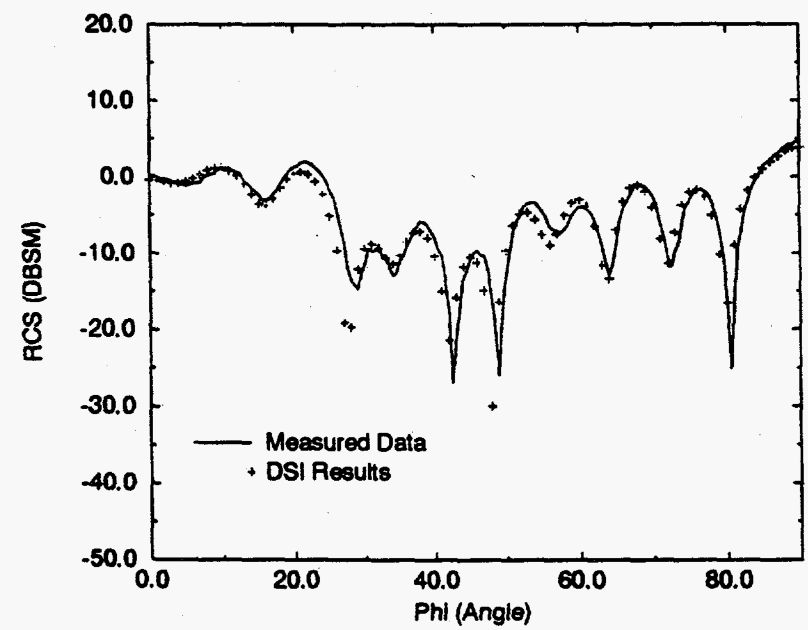

Figure 12. HH polarization cross section at 5.9 GHz for target 4, using the mesh in Figures 11 and 2.

The same input file that was used for Figure 4 is also used to obtain Figure 13.

```
local_dir     /var/tmp/t4_
start_time    0.0
num_steps     8192
dt            0.0
eps0          8.8541853367e-12
xmu0          1.2566e-06
driver_id     7
ascii_coef    0
restarts      500

driver 80.0   PHI.0 0.0 78721.56184 0.1898598 85.0 16.0 0.0 2.0 -1.0

primary_output_edges
780 915
915 930

rbc higdon_higdon  60 0.0 0.01 10.0 0.015

FARREF  0.0  0.0  0.0

FARPOL
   0.0
   90.0

FARPTS
   80.    PHI.0    0.
```

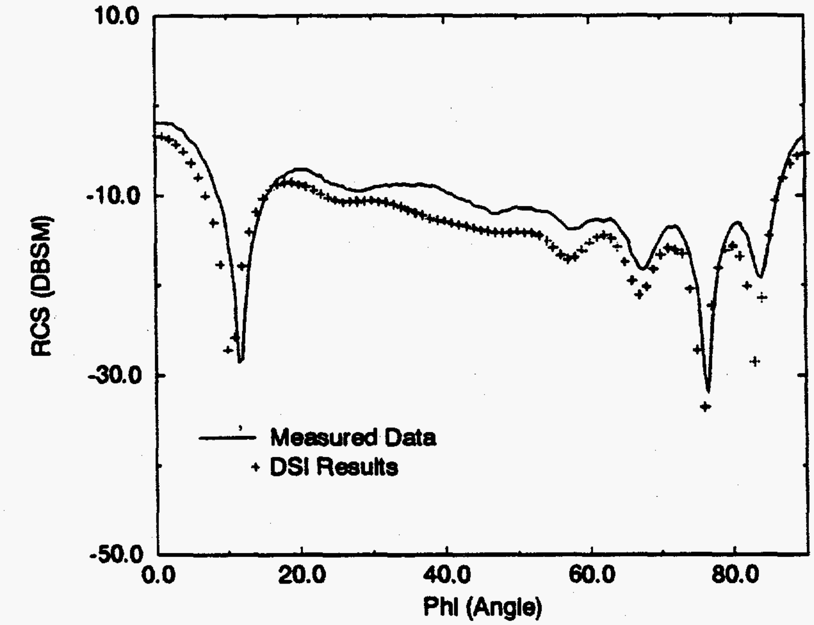

Figure 13. VV polarization cross section at 5.9 GHz for target 4, using the mesh in Figures 11 and 2.

Wedge Cylinder with Gap

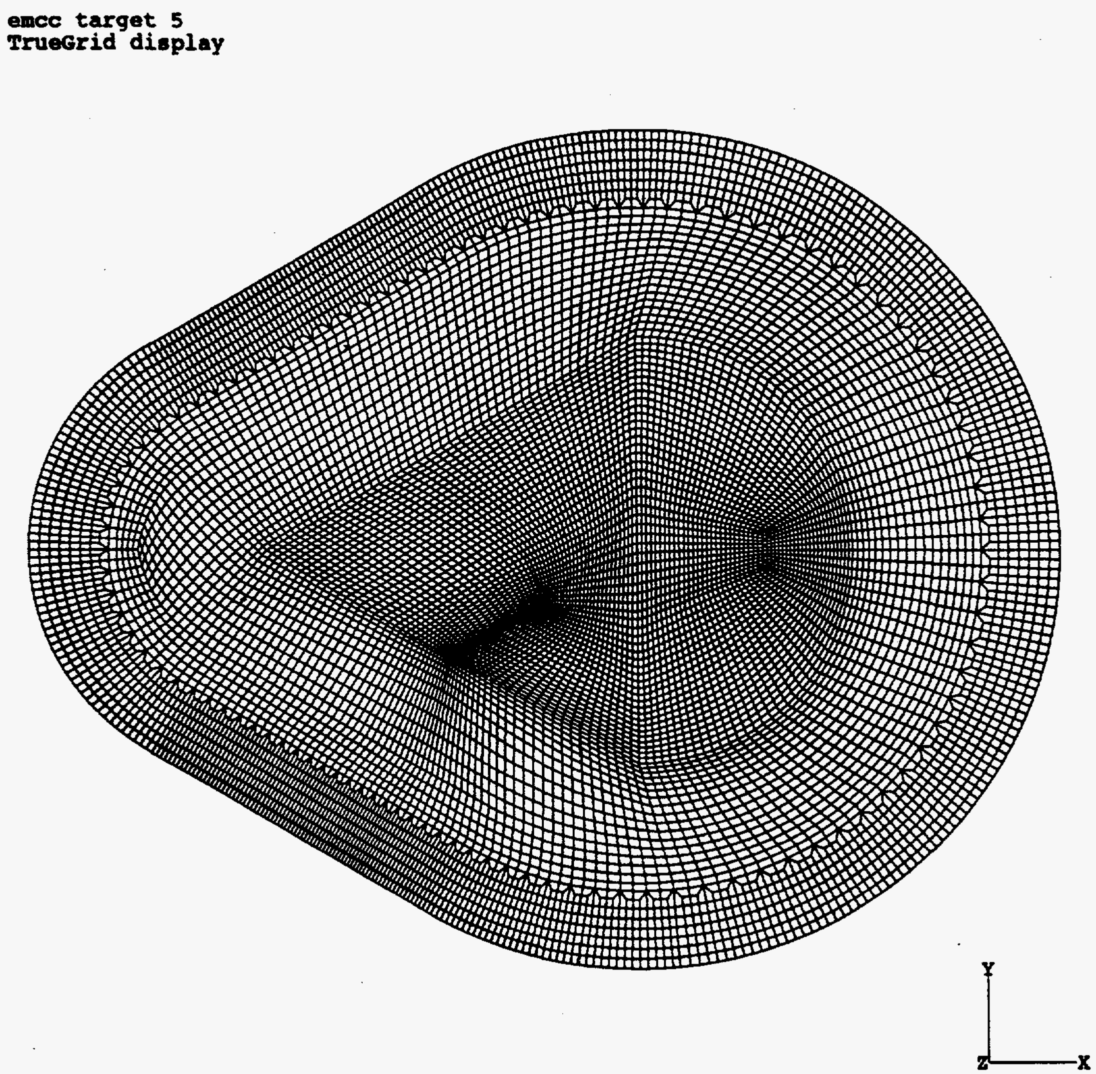

Figure 14. View of the target 5 mesh looking down the z-axis. Each cut of the mesh at a constant z coordinate in the mesh has this same appearance. See Figure 2 for the distribution of nodes in the z direction.

DSI3D was unstable on this grid. The crack width in this case is λ/100.

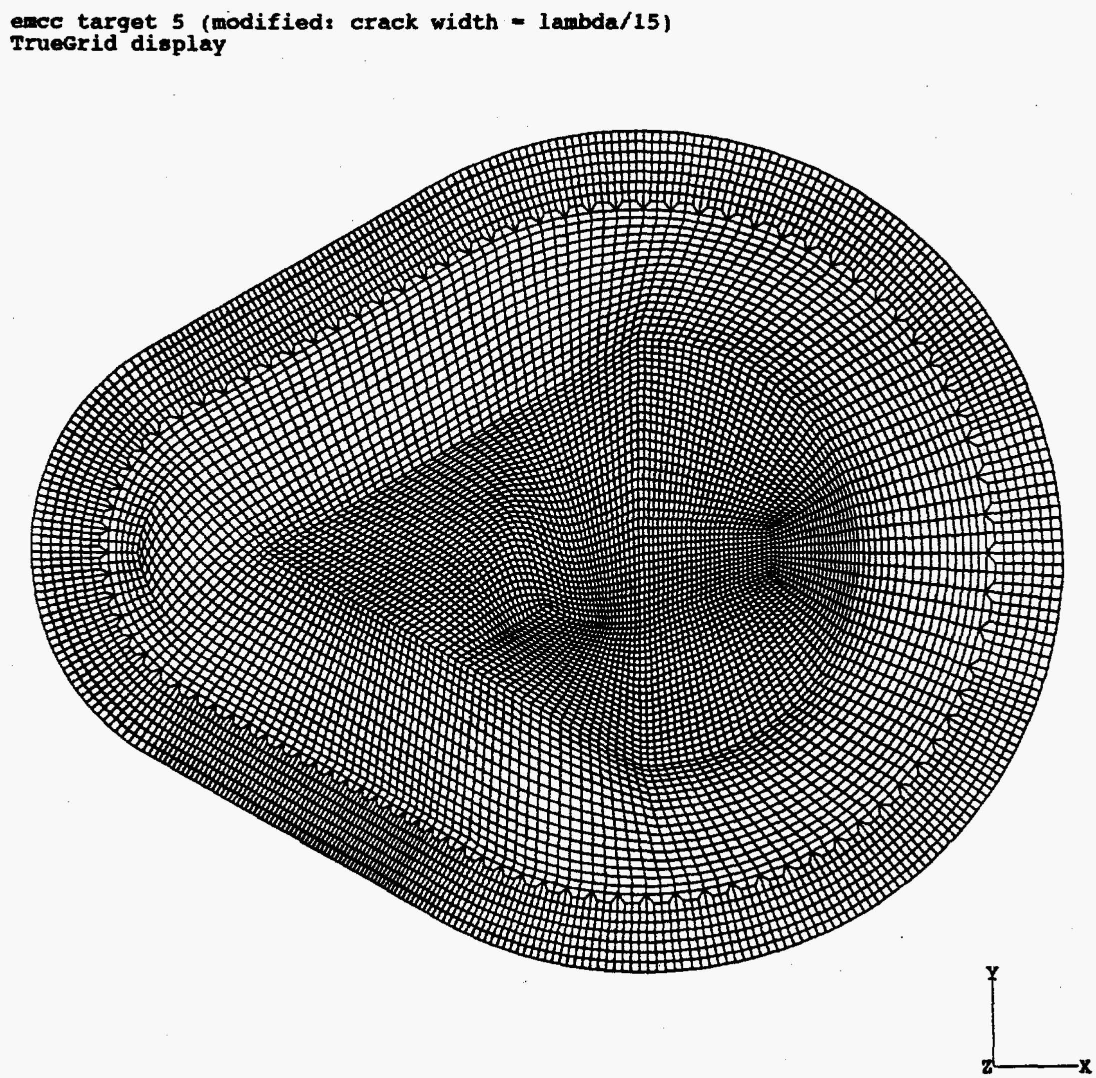

Figure 15. View of a modified target 5 mesh looking down the z-axis. The crack in this modified model is $\lambda/15$ wide. Each cut of the mesh at a constant z coordinate in the mesh has this same appearance. See Figure 2 for the distribution of nodes in the z direction.

The mesh in Figure 15 was used for the problem runs of Figure 16. The HH curve in Figure 16 was obtained with the input file that follows. The VV curve was obtained from a simple modification to the HH input file that consisted of changing the polarization of 90 degrees to 0 (zero).

```
local_dir     /var/tmp/t5_
start_time    0.0
num_steps     8192
dt            0.0
eps0          8.8541853367e-12
xmu0          1.2566e-06
driver_id     7
alpha         30
ascii_coef    0
restarts      500

driver 80.0   180.0 90.0 78721.56184 0.1898598 85.0 16.0 0.0 2.0 -1.0

primary_output_edges
780 915
915 930

rbc higdon_higdon  60 0.0 0.01 10.0 0.015

FARREF  0.0  0.0  0.0

FARPOL
   0.0
   90.0

FARPTS
   80.    180.0    0.
```

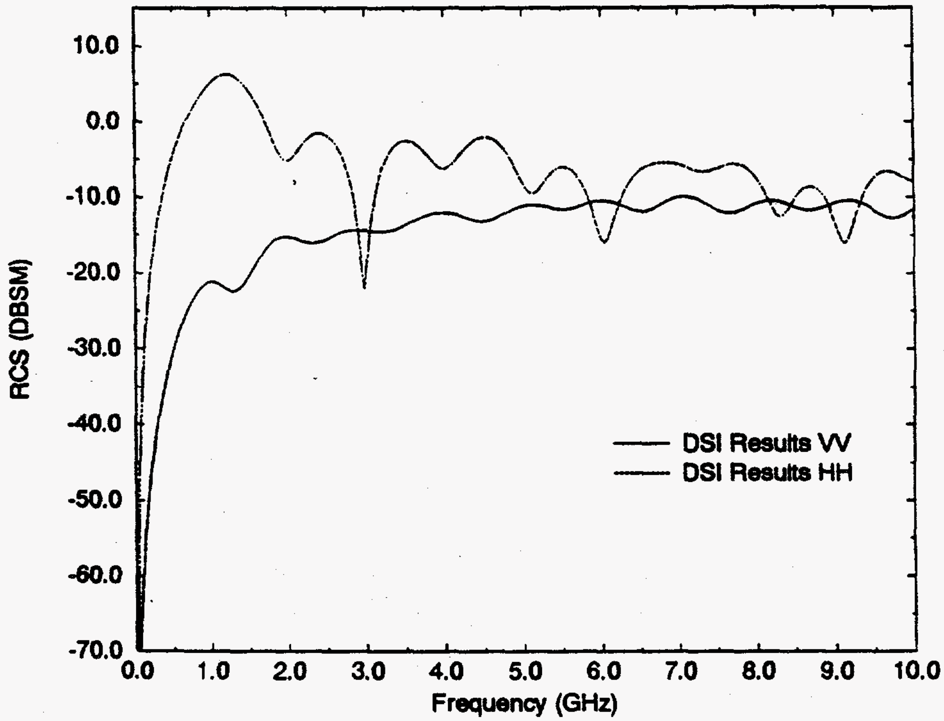

Figure 16. HH and VV polarization cross sections for target 5 with a crack width of $\lambda/15$, using the meshes in Figures 15 and 2. The angle ϕ of the incident pulse is 180°.

NASA Almond

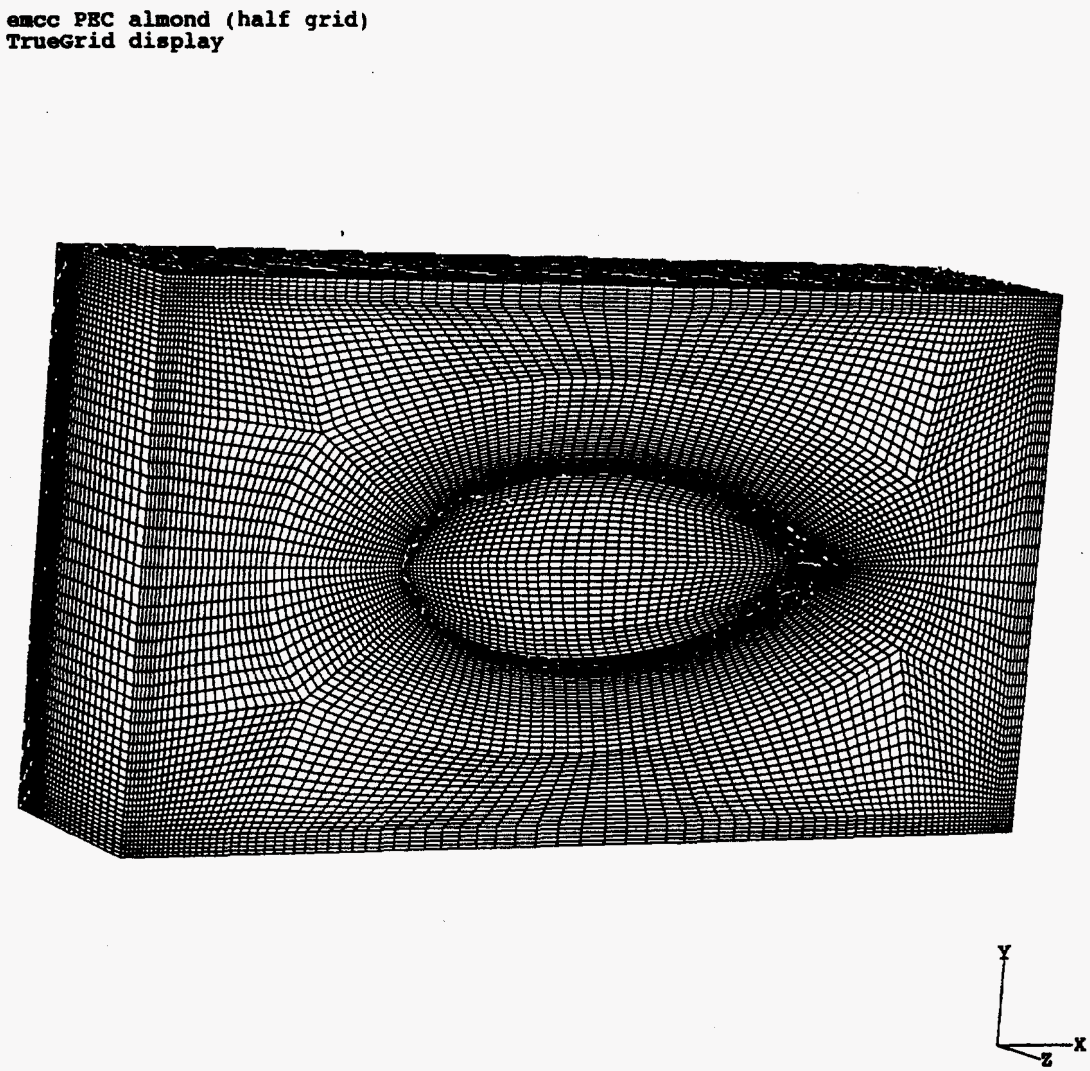

Figure 17. View of half of the PEC almond target mesh.

Figure 18 was obtained with the following input file.

```
local_dir     /var/tmp/wge_
start_time    0.0
dt            0.0
num_steps     8192
eps0          8.8541853367e-12
xmu0          1.2566e-06
driver_id     7
ascii_coef    0
alpha         30.0
restarts      1024

driver 90.0 PHI.0 90.0 78721.56184 0.15 85.0 16.0 0.0 2.0 -1.0

primary_output_edges
64091 64351
64091 64117

rbc higdon_higdon  52 0.0 0.01 0.0 0.015

FARREF  0.0  0.0  0.0

FARPOL
   0.0
   90.0

FARPTS
   90.    PHI.0
```

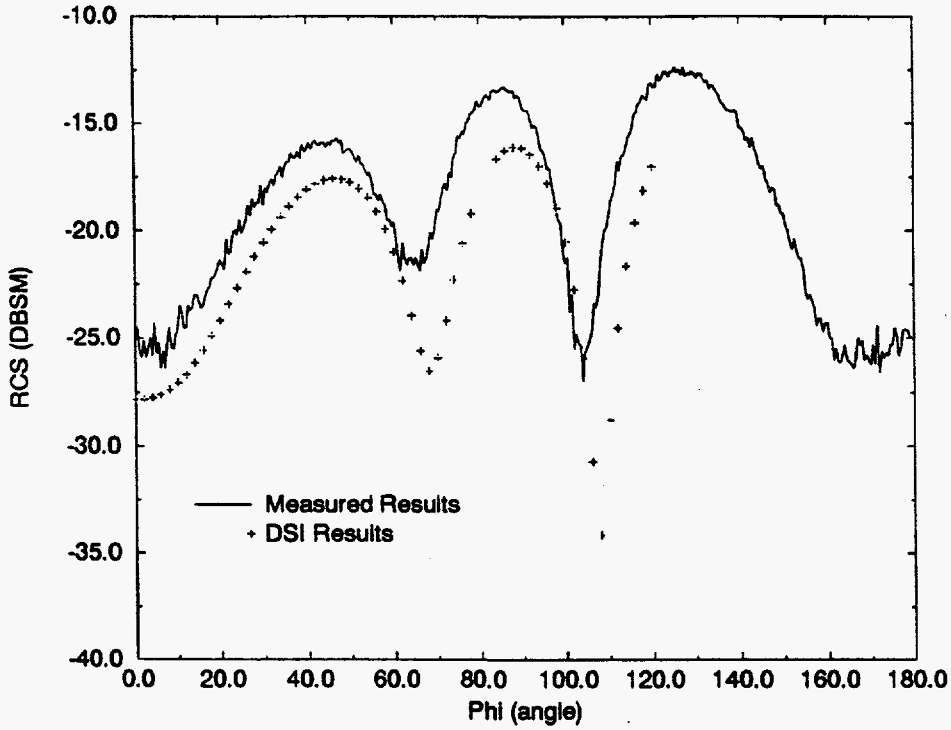

Figure 18. HH polarization cross section at 1.19 GHz for the PEC almond target, using the mesh in Figure 17.

Figure 19 was obtained with the following input file.

```
local_dir     /var/tmp/alm_
start_time    0.0
dt            0.0
num_steps     8192
eps0          8.8541853367e-12
xmu0          1.2566e-06
driver_id     7
ascii_coef    0
alpha         10.0
restarts      1024

driver 90.0 PHI.0 0.0 78721.56184 0.15 85.0 16.0 0.0 2.0 -1.0
```

```
primary_output_edges
64091 64351
64091 64117

rbc higdon_higdon  52 0.0 0.01 0.0 0.01

FARREF  0.0  0.0  0.0

FARPOL
   0.0
   90.0

FARPTS
   90.    PHI.0
```

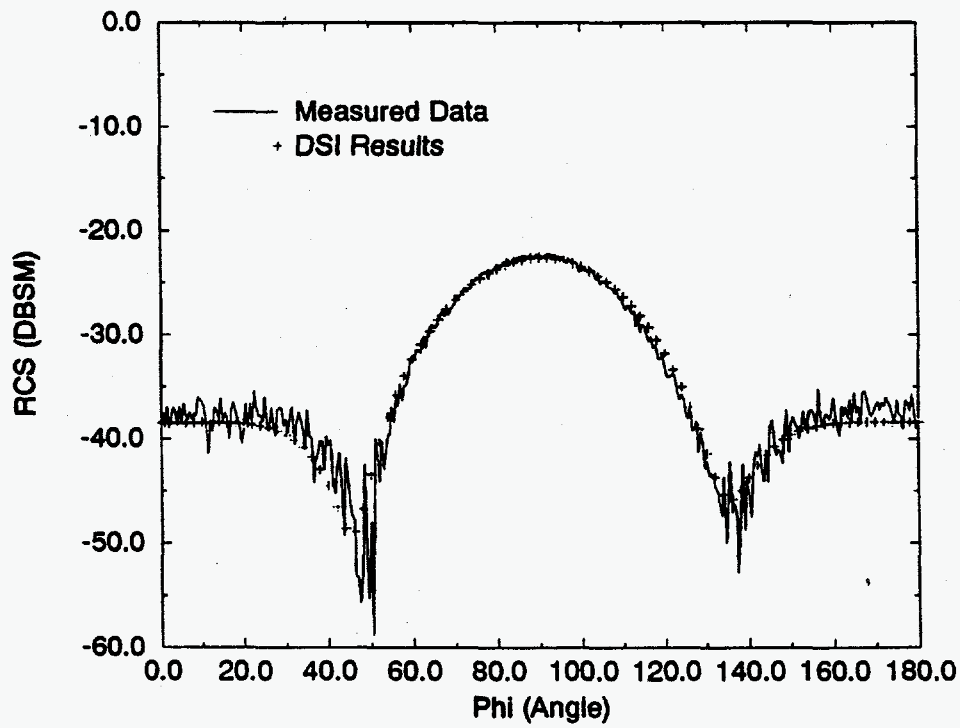

Figure 19. VV polarization cross section at 1.19 GHz for the PEC almond target, using the mesh in Figure 17.

Figure 20 illustrates the shape of the far field integration surface by showing a cut away view of that surface and the meshed surface of the PEC almond.

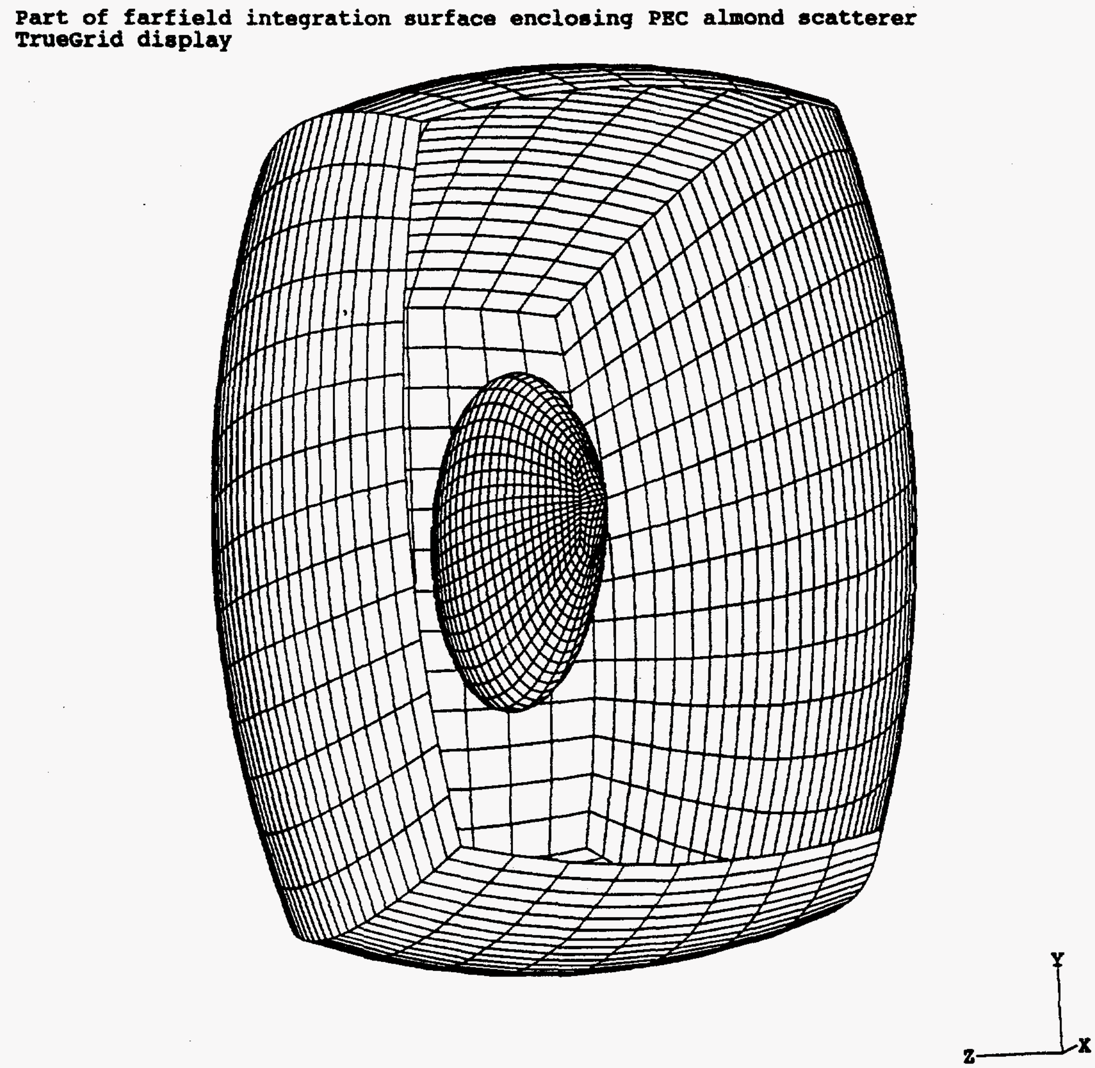

Figure 20. View of PEC almond target mesh surface surrounded by part of the mesh on the far field integration surface.

Wavelength Circular Cavity

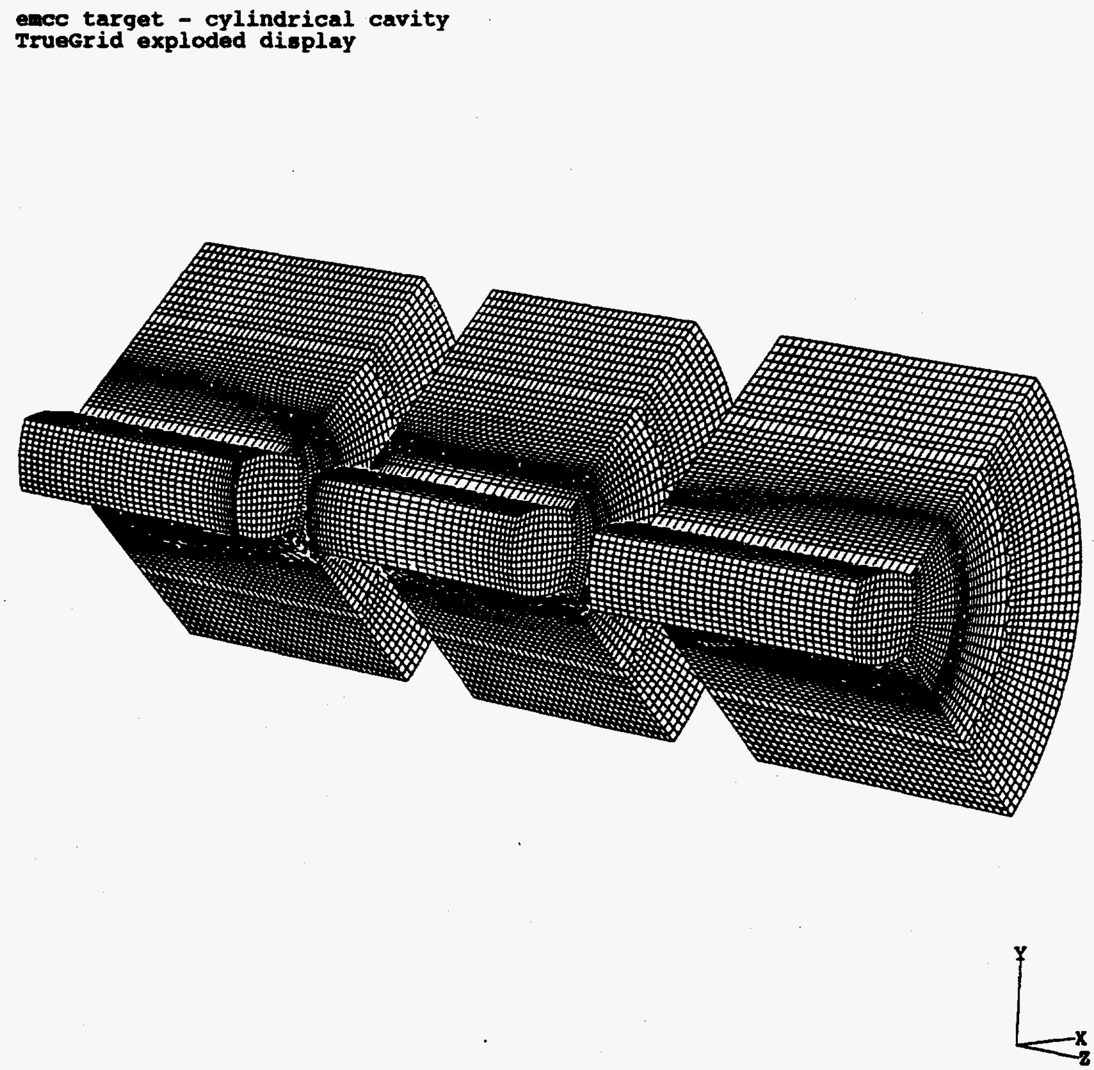

Figure 21. Cutaway and exploded view of the cylindrical cavity target mesh. The cavity is located in the middle section of the mesh and ends where the mesh is dense radially.

Figure 22 was obtained with the following input file. Note that the shell script has to be modified to use the keyword **THETA** instead of **PHI**.

```
local_dir     /var/tmp/cyl_
start_time    0.0
num_steps     8192
dt            0.0
eps0          8.8541853367e-12
xmu0          1.2566e-06
driver_id     7
ascii_coef    0
smtst         0.0004
alpha         30
restarts      1024

driver THETA.0 0.0 0.0 78721.56184 0.08 96.0 16.0 0.0 2.0 -1.0

primary_output_edges
354 353
354 349
354 384

rbc higdon_higdon  60 0.0 0.015 0.0 0.01

FARREF  0.0  0.0  0.0

FARPOL
   0.0
   90.0

FARPTS
   THETA.0    0.0
```

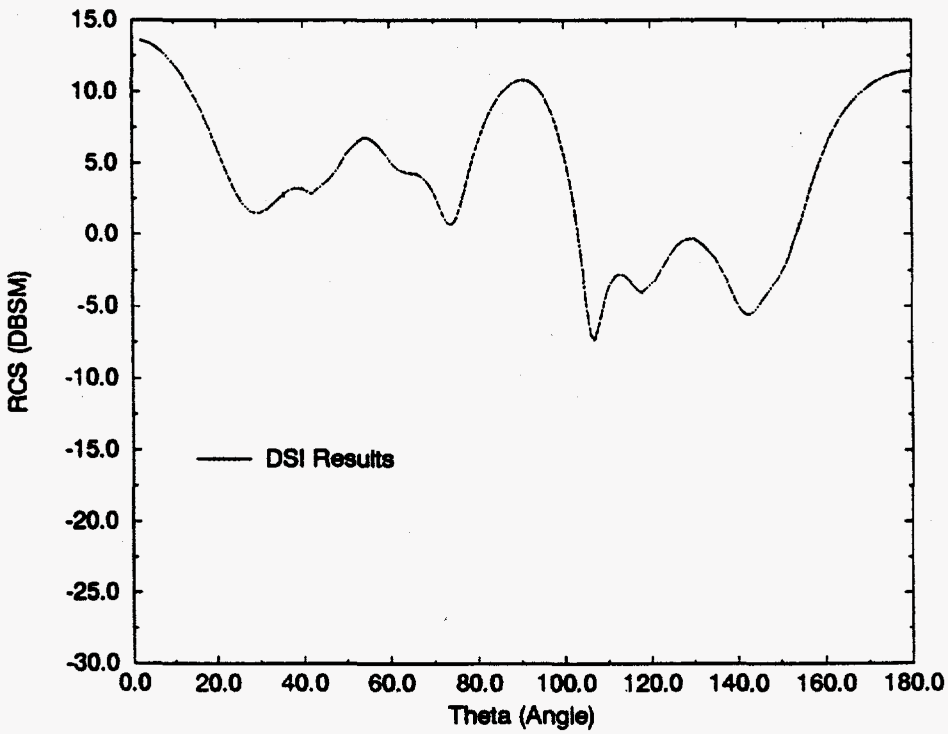

Figure 22. HH polarization cross section at 5.0 GHz for the cylindrical cavity, using the mesh in Figure 21.

Figure 23 was obtained with the following input file. Again, note that the shell script has to be modified to use the keyword **THETA** instead of **PHI.**

```
local_dir     /var/tmp/cyl_
start_time    0.0
num_steps     8192
dt            0.0
eps0          8.8541853367e-12
xmu0          1.2566e-06
driver_id     7
ascii_coef    0
smtst         0.0004
alpha         30
restarts      1024
```

```
driver THETA.0 0.0 90.0 78721.56184 0.08 96.0 16.0 0.0 2.0 -1.0

primary_output_edges
354 353
354 349
354 384

rbc higdon_higdon  60 0.0 0.015 0.0 0.01

FARREF  0.0  0.0  0.0

FARPOL
   0.0
   90.0

FARPTS
   THETA.0    0.0
```

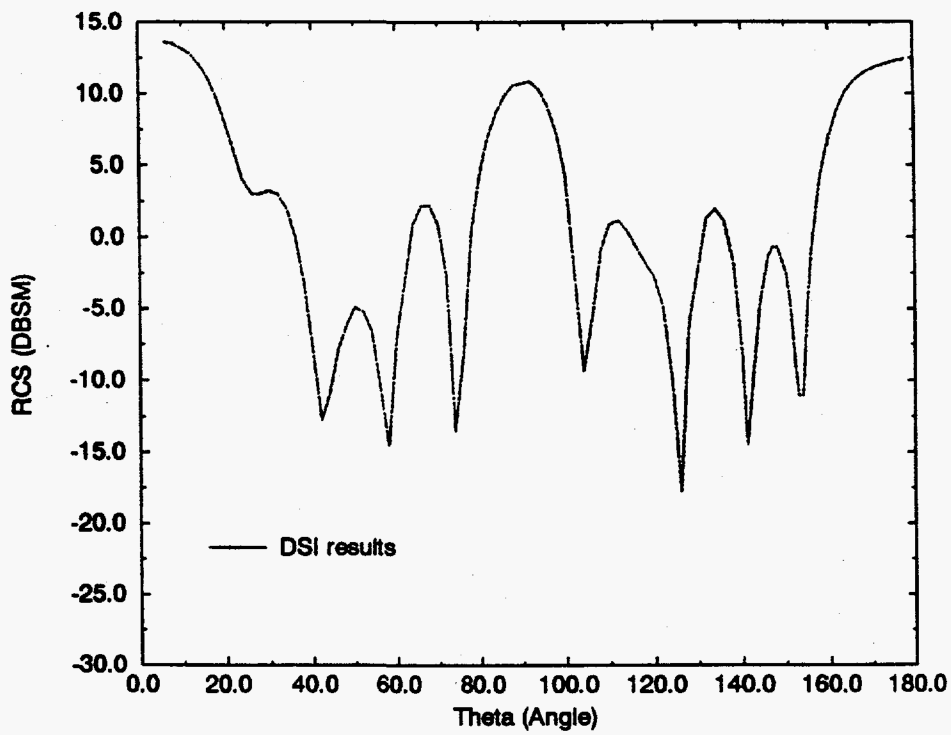

Figure 23. VV polarization cross section at 5.0 GHz for the cylindrical cavity, using the mesh in Figure 21.